Granular Matter (2012) 14:433–447
DOI 10.1007/s10035-012-0348-x

ORIGINAL PAPER

On the influence of inter-particle friction and dilatancy in granular materials: a numerical analysis

Z. X. Yang · J. Yang · L. Z. Wang

Received: 20 July 2011 / Published online: 5 April 2012

Abstract Mechanical behavior of granular soils is a classic research realm but still yet not completely understood as it can be influenced by a large number of factors, including confining pressure, soil density, loading conditions, and anisotropy of soil etc. Traditionally granular materials are macroscopically regarded as continua and their particulate and discrete nature has not been thoroughly considered although many researches indicate the macro mechanical behavior closely depends on the micro-scale characteristics of particles. This paper presents a DEM (discrete element method)-based micromechanical investigation of inter-particle friction effects on the behavior of granular materials. In this study, biaxial DEM simulations are carried out under both 'drained' and 'undrained' (constant volume) conditions. The numerical experiments employ samples having similar initial isotropic fabric and density, and the same confining pressure, but with different inter-particle friction coefficient. Test results show that the inter-particle friction has a substantial effect on the stress-strain curve, peak strength and dilatancy characteristics of the granular assembly. Clearly, it is noted that apart from the inter-particle friction, the shear resistance is also contributed to the dilation and the particle packing and arrangements. The corresponding microstructure evolutions and variations in contact properties in the particulate level are also elaborated, to interpret the origin of the different macro-scale response due to variations in the inter-particle friction.

Keywords Discrete element method · Inter-particle friction · Mechanical behavior · Dilatancy · Macro- and micro-scales · Granular materials

Z. X. Yang (✉) · L. Z. Wang
Department of Civil Engineering, Zhejiang University, Hangzhou, Zhejiang, China
e-mail: zxyang@zju.edu.cn

L. Z. Wang
e-mail: wanglz@zju.edu.cn

J. Yang
Department of Civil Engineering, The University of Hong Kong, Pokfulam, Hong Kong
e-mail: junyang@hku.hk

List of symbols

k_n, k_s	Normal and tangential stiffness of contact model
D_{50}	Mean particle diameter in a particle assemblage
σ_x, σ_y	Principal stresses along x and y directions respectively
σ_1', σ_2'	Major and minor principal stresses respectively
p, q	Mean normal stress and deviatoric stress respectively
$\varepsilon_a, \varepsilon_v$	Axial strain along y direction and volumetric strain respectively
$\varepsilon_v^p, \varepsilon_q^p$	Plastic volumetric and deviatoric strains respectively
CN	Coordination number
φ_μ, μ	Inter-particle friction angle and inter-particle friction coefficient
d_{ij}, δ_{ij}	Second order deviatoric tensor and Kronecker delta
n_i	Direction cosines of the unit vector with respective to the reference axes x_i
$E(\varphi), E_0$	A density function and mean value of the density over direction respectively
Δ_d, φ_d	Intensity and principal direction fabric tensor in general
$r(\varphi), r_0$	Spatial distribution of quantity r and its mean value over direction respectively

Δ_d^r, φ_d^r	Intensity and principal direction fabric tensor in term of quantity r
$f_n(\varphi)$, f_0	Normal contact force distribution and mean value of normal contact force respectively
$f_t(\varphi)$	Tangential contact force distribution
Δ_d^n, φ_d^n	Intensity and principal direction of fabric tensor in terms of contact normal force
Δ_d^t, φ_d^t	Intensity and principal direction of fabric tensor in terms of contact tangential force
$f_\mu(\varphi)$	Mobilized inter-particle friction distribution
$\Delta_d^\mu, \varphi_d^\mu$	Intensity and principal direction fabric tensor in terms of mobilized inter-particle friction
ϕ_{mob}	Mobilized friction angle
η, η_{res}	Mobilized stress ratio and stress ratio at residual state respectively
$A.R.$	Aspect ratio of particle characterizing the particle's shape

1 Introduction

Mechanical behavior of granular soils is very complex and can be influenced by various factors, including confining pressure, density, fabric, loading conditions, etc. [1–7]. Recent investigations [8–10] also indicate the mechanical behavior (such as shear resistance) could be significantly affected by the particle level's characteristics, such as particle shape (angularity, roundness and sphericity), particle surface characteristics, gradations of particles, etc., which reflect the chemical, physical, and biological environmental evolutions in the geological process.

Among the mechanical behaviors, dilatancy is one of the essential characteristics of granular soils and of significance in academia as well as in engineering practice. When subjected to shearing, a loose sand contracts and dense sand dilates, governed by both the stress ratio and inter-particle friction in terms of Rowe's stress-dilatancy equation [11]. The shear strength stems from the inter-particle friction and the resistance against the volumetric dilation of the particle assembly. Microscopically, the volumetric deformation of the granular assembly upon shearing (i.e. dilatancy) is largely attributed to particle motion and rearrangement in the manner of sliding and/or rolling, if no particle breakage occurs. From the particle scale's perspective, it is interesting to explore how the inter-particle friction influences the motion of the particles and then the macro-mechanical behavior of granular soils.

Experimental work has been reported to justify the dependence of mechanical response on the particle characteristics. Skinner [12] suggested that the inter-particle friction does not significantly change the shear strength of granular materials under plane strain conditions, while Haruyama [13] showed that shear strength and dilatancy increased with increasing surface roughness of granular particles in triaxial compression tests. And Procter and Barton [14] further pointed out that the inter-particle friction is a function of mineral composition, surface chemistry, as well as the shape and surface roughness of the granular particles. Recently Cavarretta et al. [15] established a correlation between inter-particle friction and roughness by directly measuring particle roughness and inter-particle friction. Interestingly, however, macro-scale experimental tests [16–18] indicated that the influence of particle shape is much more noticeable than that of surface roughness (or inter-particle friction).

Over the past decades, DEM (discrete element method)-based numerical analysis has prevailed in the investigations of mechanical behavior of granular soils, including the influences of particle characteristics, typically inter-particle friction and particle shape. DEM simulation treats the granular material as an assembly of particles that interact via a contact logic and can offer a thorough perspective of the response at the particulate level as well as the overall behaviors. Jensen et al. [19] demonstrated the particle rotations and the shear strength greatly depends on the particle shape. Polygonal particles are also used to investigate the influence of particle shape on the mechanical behavior both in macro- and micro-scales, see [20–22]. Thornton [23] showed both the peak and critical state friction angles increase with the coefficients of inter-particle friction μ when $\mu \leq 0.5$, while Powrie et al. [24] indicated a significant dependence of peak strength on the inter-particle friction in the range of $0.7 \geq \mu \geq 0.3$ but only modest increase in the residual strength based on triaxial test simulation. Alonso-Marroquín et al. [25] also observed independence of the mobilized friction angle at the critical state of the inter-particle friction, and this non-dependence was attributed to the spontaneous formation of rotational patterns and clusters of particles with intense rolling. Peña et al. [22] presented the similar results of the investigation of the effect of inter-particle friction on the macro-mechanical behaviour of granular materials, using convex polygonal particles. Other DEM simulations [26–28] imply that the inter-particle friction may influence the macroscopic response, including the dilatancy characteristics of granular materials.

Although the macro-mechanical behavior of granular soils has been well examined by laboratory experiments and numerical simulations as summarized above, the micro-scale analysis has not been adequately addressed to provide a clear insight into the mechanisms and the significance of the inter-particle friction. This paper presents extensive numerical investigation into the influence of inter-particle frictions on the mechanical behavior of granular assembly based on DEM analysis. The numerical samples all have similar initial isotropic fabric and density, and the same confining pressure, but with different inter-particle friction coefficient. A series of numerical 'experiments' (simulations) are carried out under

both drained and undrained conditions. The dilatancy and the shear failure modes of samples with varying inter-particle frictions can be identified and quantified. Comparisons are also made to Rowe's stress-dilatancy formulations, to take into account the effect of the inter-particle friction. It has also shown that the micromechanical analysis can be linked with and interpreted into the macro-scale responses that due to variations in the inter-particle friction.

2 DEM Model

DEM assumes the material consisting of separate, discrete particles and is particularly capable of describing the micro-mechanical behavior of granular assemblies. In this paper, a commercial code PFC^{2D} (Particle Flow Code in two dimensions) (Itasca, 2005) based on the distinct element method proposed by Cundall and Strack [29] is employed. In the code, an explicit time-stepping numerical scheme is implemented and the motion of individual particles is traced and contacts with neighboring particles are updated according to a particular contact law. A detailed description on the theory and background can be referred to Cundall and Strack [29].

For a granular assembly simulated with PFC^{2D}, the particles are assumed as rigid bodies and are interacting through the contacts in the micro-scale. As the contacts are simulated as a soft contact model with a specified contact force-deformation relationship, the deformation of the assembly can still be allowed to take place at the contacts. The contact law used in this study is a spring-slider model with two portions: bi-directional (normal and tangent) linear spring model and tangent Coulomb-type slip model. The former states a linear elastic relationship between contact force and contact deformation, both in normal and tangential directions, while the latter ensures a Coulomb type friction mechanism between the normal and shear forces at contact points. In addition, as PFC^{2D} solves a pseudo-static problem by solving a set of motion equations, damping is introduced to eliminate the non-steady kinetic energy.

All the parameters used in the numerical simulation are commonly used in literature or default values of *PFC*, and are summarized in Table 1. The wall stiffness is assigned to be the same as the particles, while the friction between walls and particles is set to zero, signifying the boundary particles can move freely along the walls.

3 Numerical sample

In recent years, some algorithms and techniques for the generation of numerical samples have been developed for DEM analysis (e.g. [30–33]). Among them, both expansion method and deposition method have the advantage over others in less effort in computation, well control of desired particle gradation and readily achieving a specified initial density. Generally, the expansion method can produce an initially isotropic sample while the deposition method tends to introduce certain inherent anisotropy into the microstructure of the sample [34,35]. The expansion method was adopted here to generate samples such that the influence of the initial anisotropy effect can be isolated. The dimension of the sample is 25 mm × 25 mm.

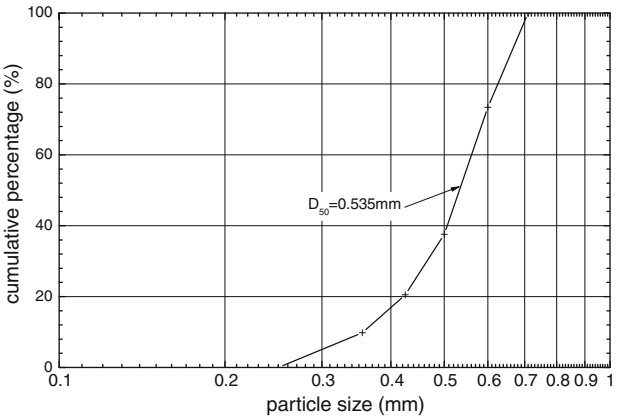

Fig. 1 Grading curve of the numerical sample

In the PFC^{2D} model, the basic circular disk elements range from 0.26 to 0.66 mm in diameter with $d_{50} = 0.535$ mm, as shown in Fig. 1. Noting that the circular particle elements may lead to over-loosening the restriction of particle rolling during the loading process and then inevitably affect the dilatancy and deformation of the granular assembly [36–38], a spindly clumped element [39] shown in Fig. 2 is used in this study. Some previous discrete element simulations [20–22,40,41] have shown that using non-circular(oval or polygonal) particles can also reduce the particle rolling greatly. The clumped element is formed by glueing and overlapping two identical basic disk particles and behaves as a rigid body that will not break apart, regardless of the forces acting upon it, and can be implemented within an existing DEM framework without the introduction of new contact or force algorithms. A parameter, aspect ratio $A.R.$, is defined to characterize the shape of clumped particle as shown in Fig. 2. The variation of $A.R.$ values is bounded by two extreme cases: $A.R. = 1.0$ when two disks are fully overlapped, and $A.R. = 0.5$ when two disks only contact without any overlapping. However, it is clarified that convex polygonal particle with $A.R. = 1.0$ can also restrict the particle rotation and simulate more realistic behavior of granular materials, see Peña et al. [22].

Once the sample has been generated, an isotropic small confining stress 10 kPa is applied and the sample thus has an initial effective stress = 10 kPa. After that, a compaction procedure is implemented to achieve the specified stress

Table 1 Parameters used in numerical simulations

Mass density	Normal/tangential stiffness of particle/wall	Particle/wall friction	Damping parameter
2,600 kg/m^2	10^9 N/m	0	0.7

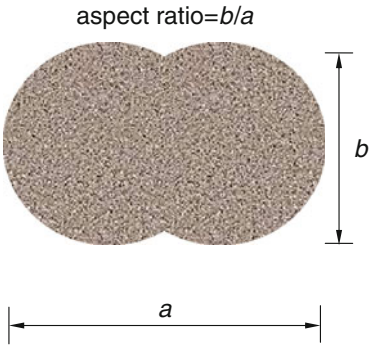

Fig. 2 A clumped particle element

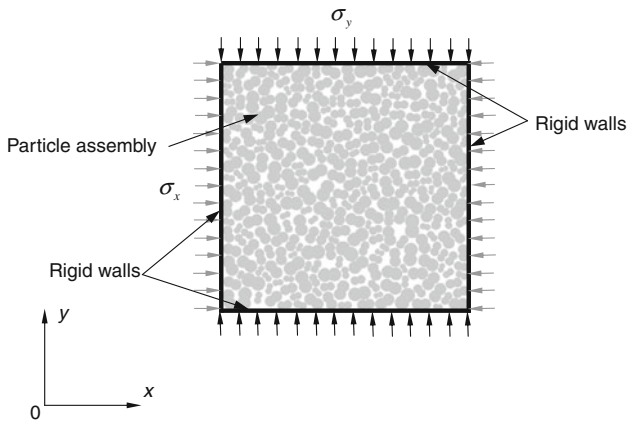

Fig. 3 A numerical sample with boundary conditions

state. Then, biaxial compressive shear under 'drained' or 'undrained' condition is proceeded. For 'drained' simulation, both the upper and lower boundary walls are pushed inwards the sample with a very small loading rate, while maintaining a constant horizontal stress (lateral confining stress) by moving the lateral walls inwards or outwards as required. The 'undrained' simulation is conducted under constant volume conditions during the course of shearing. Figure 3 illustrates a biaxial test sample with imposed boundary conditions.

4 Numerical biaxial shear test

In order to investigate the influence of inter-particle friction on the mechanical behavior of the granular materials upon shearing, a series of numerical biaxial tests are conducted under both drained and undrained conditions. It is known that the particle shape also plays an important role on the behavior of particles, and some discrete element simulations (DEM) were presented previously by Ng [40] and Shodja and Nezami [41] and Nouguier-Lehon et al. [20] and Peña et al. [21,22], using oval particles and polygonal particles respectively. Alternatively in the current study, to restrict particle rolling and simulate more realistic behavior of granular materials, clumped particles with an aspect ratio of 0.6 are used in the simulation, as defined in Fig. 2. All the test specimens are compacted to the same isotropic stress state with an initial confining pressure of 1,000 kPa and expected to possess an isotropic microstructure. This is justified by the distributions of particle orientation, contact unit normal, branch vector and the contact force network shown in Fig. 4 for a specimen after the isotropic compaction, with dotted lines indicating the Fourier approximation (the variables' definitions and representations can be found in the Appendix). To investigate the influence of inter-particle friction, five different target inter-particle friction coefficients of 0.05, 0.10, 0.20, 0.50 and 1.0 are considered. To highlight this influence and make the simulation results more comparable, all the numerical specimens have close initial void ratio (in a narrow range of $e = 0.15 \sim 0.17$) before shearing. Based on some trial tests to control the density of the samples by varying inter-particle friction coefficient μ_{pre} during the preparation, it is noted that at the reference state $p' = 10$ kPa, maximum void ratio is $e_{\max} = 0.257$ ($\mu_{\text{pre}} = 0.5$) and minimal void ratio $e_{\min} = 0.136$ ($\mu_{\text{pre}} = 0.0$). Thus initial void ratio at $p' = 1,000$ kPa in this test is around $0.15 \sim 0.17$ and ralitative density $D_{\text{r}} = \sim 80$ %, and the samples are considered as very dense.

In the two dimensional analysis, the mean normal stress and deviatoric stress are defined as $p' = (\sigma'_x + \sigma'_y)/2$ and $q = \sigma'_y - \sigma'_x$, where σ'_x and σ'_y are principal values along x and y directions respectively (Fig. 3). Figure 5 gives the biaxial shear test results with different inter-particle friction coefficients under drained condition. As shown in Fig. 5a, the samples with $\mu \geq 0.5$ exhibit significant volumetric dilation, while those with $\mu < 0.2$ behave in a contractive fashion. This suggests the inter-particle friction notably influences the dilatancy response for granular soils. The underlying mechanisms may be that: a small friction facilitates the repacking and rearrangement of the particles during the shearing and results in a contractive volume change; on the other hand, large friction may tend to partially hinder the motion of particles and the inter-particle sliding is less likely to occur, therefore the specimen tends to dilate, in response to the application of the deviatoric load.

Figure 5b presents the evolution of the stress ratio q/p' as the axial strain ε_a increases, where the axial strain denoting

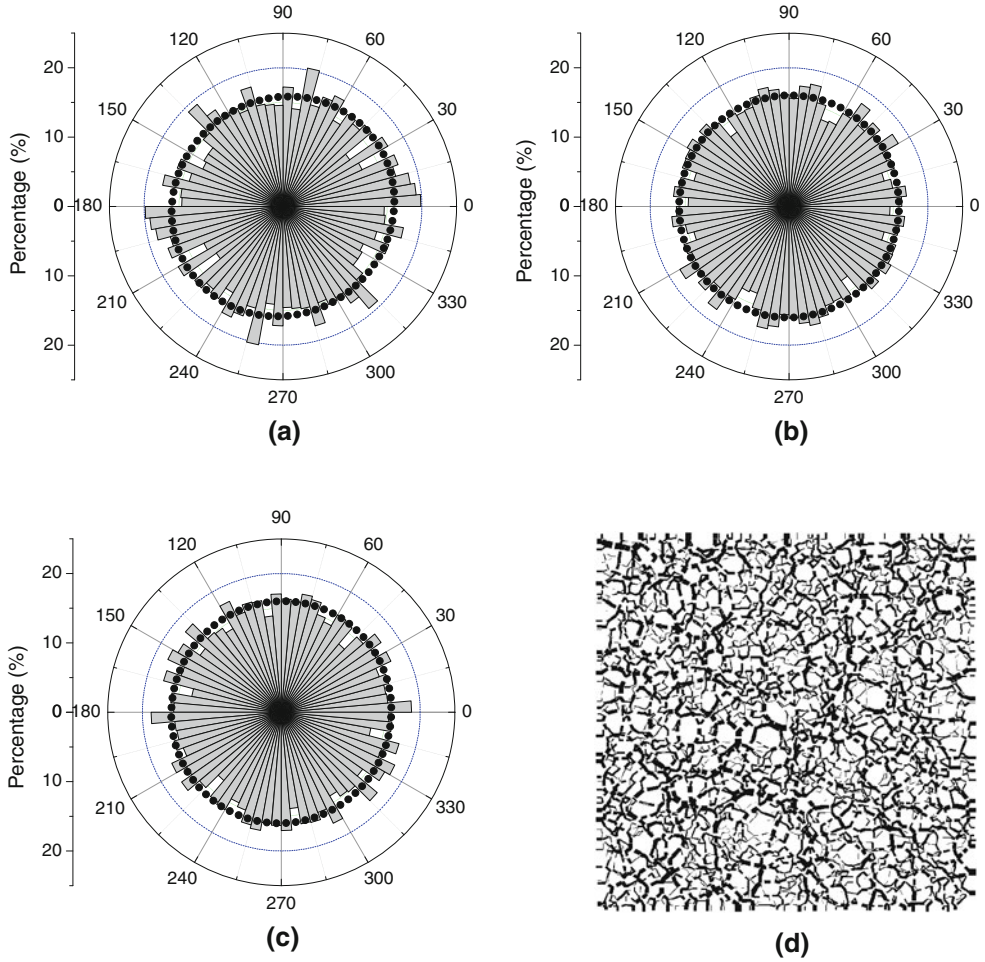

Fig. 4 An isotropic specimen after compaction. **a** particle orientation, **b** contact normal, **c** branch vector orientation, **d** contact force network

strain along y direction. It is seen that for the cases with $\mu = 0.5$ and 1.0, q/p' reaches the peak values at $\varepsilon_a \approx 2$ % and then drops as ε_a increases, while the cases with $\mu \leq 0.2$ exhibit hardening stress-strain responses. However, critical state values of q/p' for the cases with $\mu \geq 0.2$ are marginally influenced and tend to approach a common value ≈0.8. It is also interesting to note that for the cases with $\mu \leq 0.10$, the critical values of q/p' are not far smaller than those with higher inter-particle frictions, indicating that inter-particle friction is not the only constituent for granulates in resisting the shear loading. Noting that at the critical state, the materials are turned to be purely frictional, and apart from the inter-particle frictions, particle rearrangement and repacking are also readily formed to counter-resist the shear load [36,37].

Figure 5c illustrates the change of the void ratio against the deviatoric stress. Again, the inter-particle friction dependence of peak shear strength for higher friction cases can be observed, although the critical shear strength is not very much affected. It is also noted that the higher friction may bring the specimen to the critical state with a larger void ratio. Noting that for engineering application, mobilized friction angles at both peak and critical states are key engineering design parameters, Fig. 5d shows the mobilized friction angles, ϕ_{mob} against various inter-particle frictions, μ, where $\phi_{\text{mob}} = \sin^{-1}[(\sigma_y - \sigma_x)/(\sigma_y + \sigma_x)]$. It is seen that the peak friction angles does exist for the cases with $\mu \geq 0.5$, whereas critical state friction angle is just slightly different for all cases.

Figure 6 presents the simulation results under undrained conditions. As can be seen in Fig. 6a, the stress paths with different friction coefficients are different from one another. For cases with $\mu \leq 0.2$, the samples behave in a contractive manner and both the mean normal stress and deviatoric stress reduce during shearing, even down to a zero stress state for the cases with $\mu = 0.05$ and 0.1, which is very similar to the liquefaction state defined in saturated soils. For those with higher frictions, the specimen more likely tends to dilate to a higher stress level, and there is much less contractive behavior observed on the stress paths. Figure 6b demonstrates the stress ratios, q/p' varies with axial strain ε_a for various friction coefficients. At $\varepsilon_a \approx 2$ %, q/p' reaches the peak values

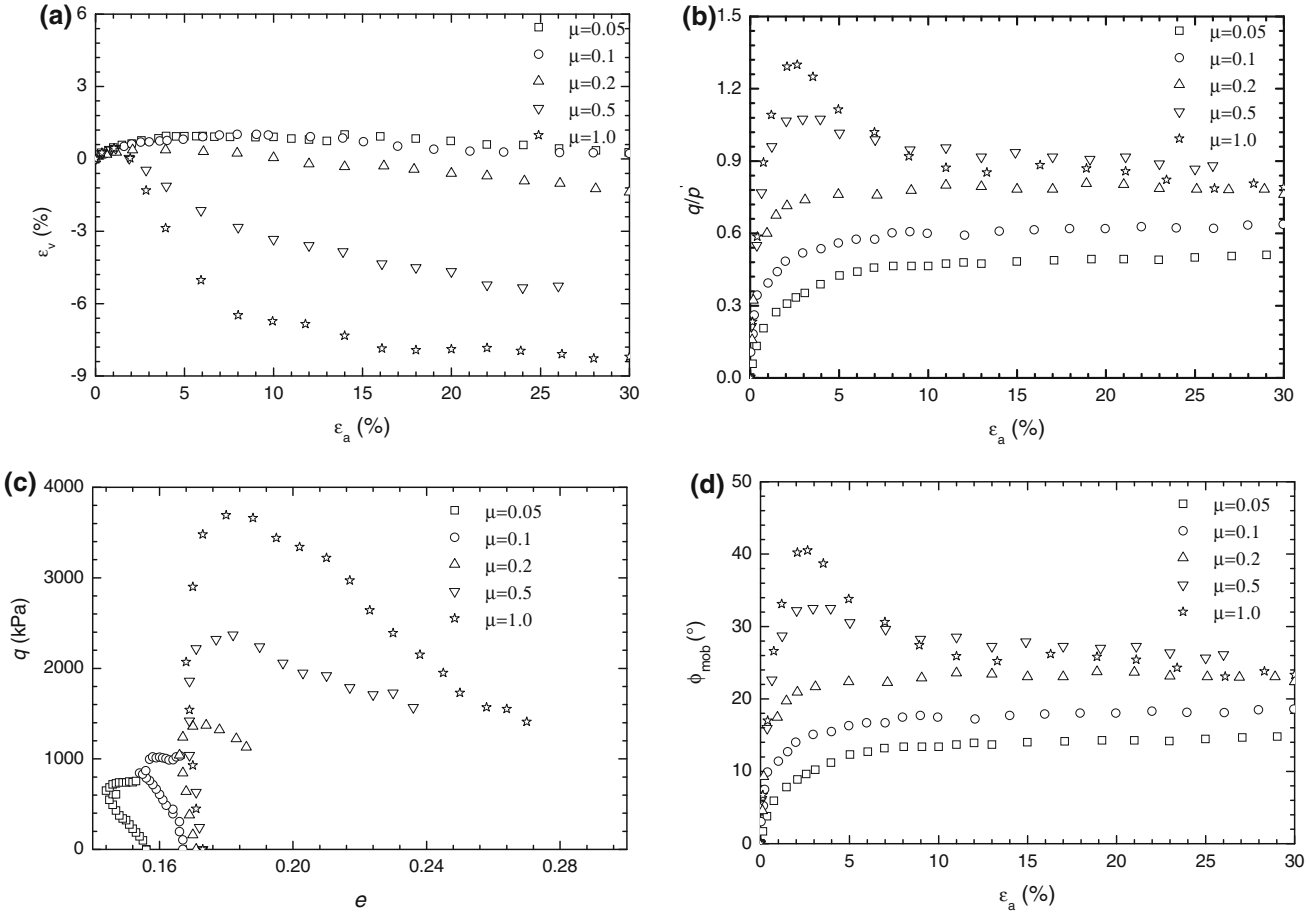

Fig. 5 Drained biaxial shear with various inter-particle frictions. **a** $\varepsilon_v \sim \varepsilon_a$, **b** $q/p' \sim \varepsilon_a$, **c** $q \sim e$, **d** $\phi_{\text{mob}} \sim \varepsilon_a$

and then drops to residual value ~0.8 for $\mu \geq 0.5$ while flattens off for $\mu \leq 0.2$. An alternative view on the variation of the mean normal stress with the axial strain is presented in Fig. 6c. Presented in Fig. 6d is the mobilized friction angle, ϕ_{mob}. For cases with $\mu = 0.5$ and 1.0, ϕ_{mob} increases to the peak values of about 34° and 40° at $\varepsilon_a \approx 2$ %, respectively, and then reaches the residual value of about 24° at $\varepsilon_a \approx 20$ % for both. However for $\mu < 0.2$, no clear dilatation is observed. The findings are quite similar to those of drained conditions.

5 Influence of overall behavior

To further examine the effect of inter-particle friction on the dilatancy response, Fig. 7 presents the relationship of the stress ratio versus the dilatancy, where the stress ratio is normalized by the corresponding stress ratio at the critical state, and the dilatancy is expressed as $d\varepsilon_v/d\varepsilon_1$. As the elastic part is relatively small, no attempt was made to differentiate the plastic from the total strain. It is clearly shown that with smaller inter-particle frictions, the granular assembly tends to contract till the critical state, while the contractive behavior with higher inter-particle frictions is much more inhibited, and the dilative response is becoming dominant after passing the phase transformation state.

To better illustrate the significance of inter-particle friction on the shear failure and dilatancy, Fig. 8 shows three typical undrained stress paths A, B and C, for different inter-particle frictions with $\mu_a > \mu_b > \mu_c$. It is seen curve A exhibits highly dilative shear failure, while curve C shows completely contractive shear failure, with curve B in between. It is noted that for a given stress ratio q/p', dilatancies D of points a, b and c on the curves are different, with $D_a < D_b < D_c$. Recalling the famous Rowe's stress-strain dilatancy equation [11], $d\varepsilon_v^p/d\varepsilon_1^p = 1-(\sigma_1'/\sigma_2')/\tan^2(45°+\varphi_\mu/2)$, where $D = d\varepsilon_v^p/d\varepsilon_1^p$ is a measure of dilatancy; σ_1'/σ_2' is the ratio between the major and minor principal stresses; φ_μ is the inter-particle friction angle, an increase in the inter-particle friction will result in a more contractive response (D increases). It is apparent that the Rowe's dilatancy equation fails to predict the dilative behavior of granular materials with higher inter-particle friction and the influence of the inter-particle friction on the dilatancy is not appropriately reflected.

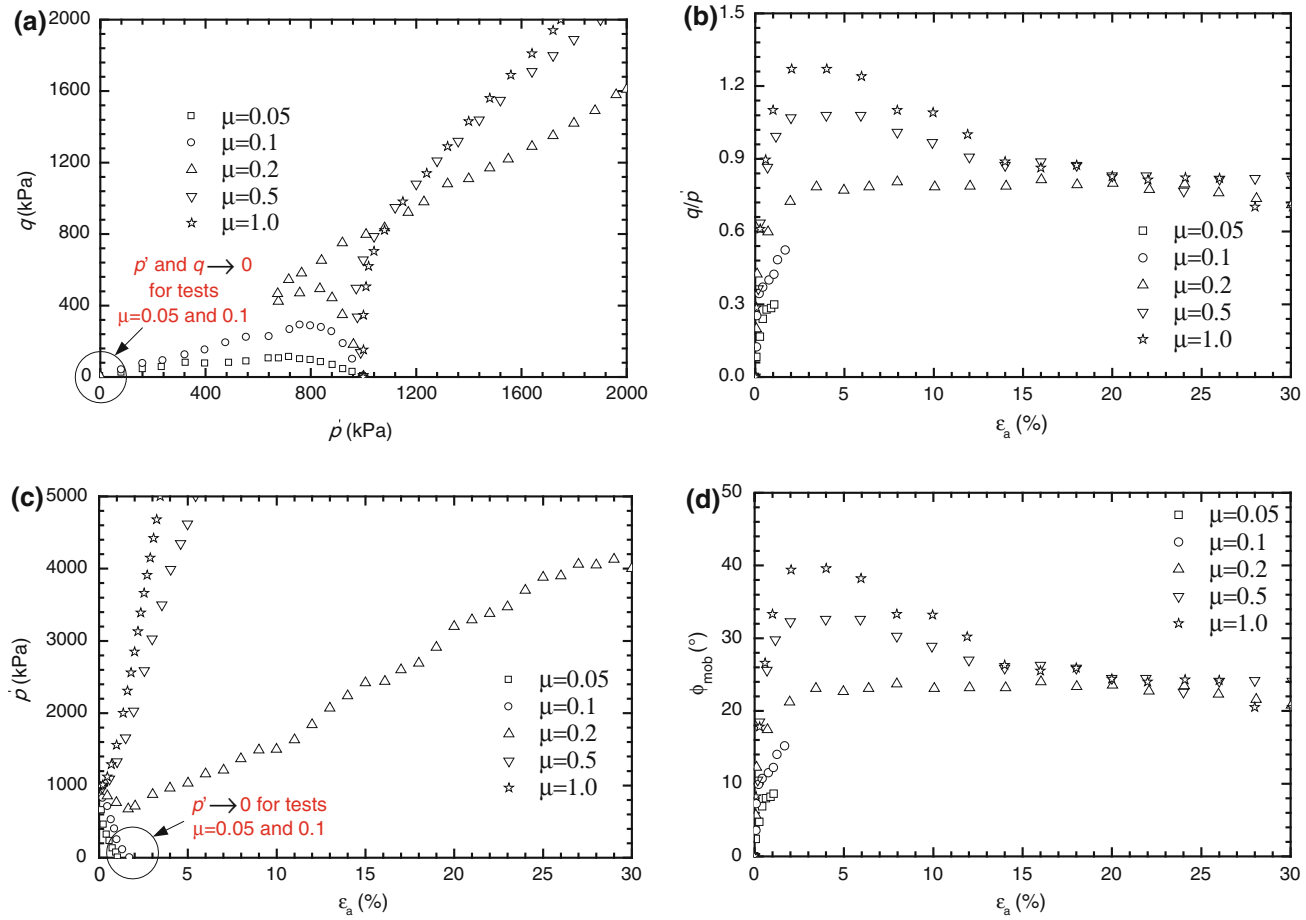

Fig. 6 Undrained biaxial shear with various inter-particle frictions. **a** $p' \sim q$, **b** $q/p' \sim \varepsilon_a$, **c** q $\sim \varepsilon_a$, **d** $\phi_{\text{mob}} \sim \varepsilon_a$

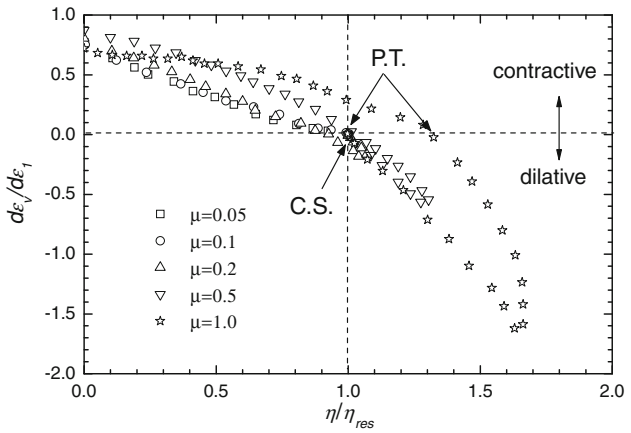

Fig. 7 Stress-dilatancy paths with various inter-particle frictions

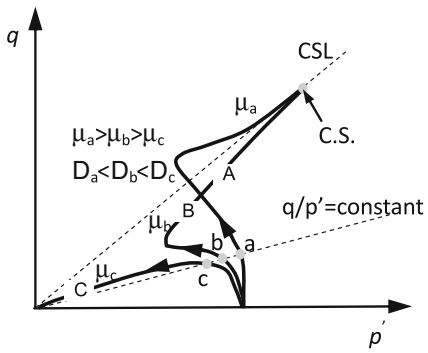

Fig. 8 Illustration of the inter-particle friction on the shear failure and dilatancy

DEM simulations conducted by Thornton [23] using PFC^{3D} with sphere elements suggest that both the peak stress ratio and critical state stress ratio depended on the inter-particle friction, but this effect is limited for $\mu \geq 0.5$ or so. The results shown in this study with clump particles are generally consistent with his conclusion, but the critical state stress ratio is fairly not affected by the friction for both the drained and undrained conditions with $\mu \geq 0.2$. This is in agreement with the experimental results by Skinner [12], in which shearing on wet and dry assemblies (with distinct inter-particle frictions) of glass ballotini gives almost identical stress ratio at critical state.

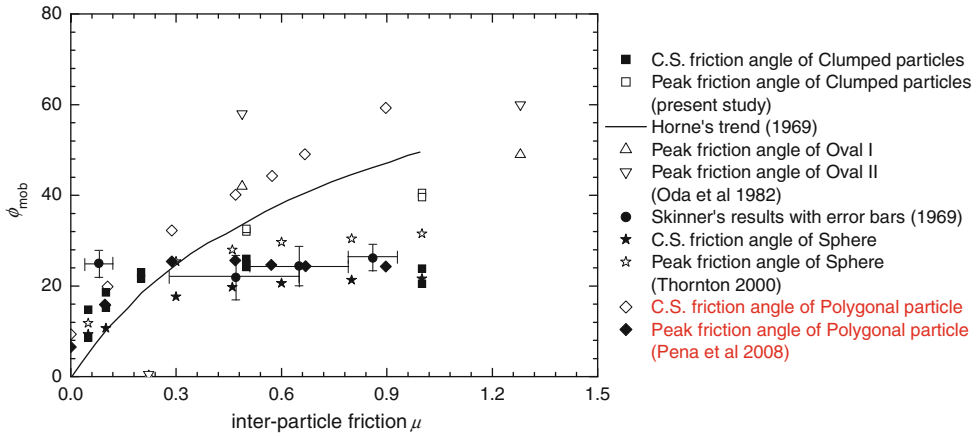

Fig. 9 Comparison of mobilized friction angles

Oda et al. [42] conducted biaxial compression testing on the assemblies of oval cross-sectional rods with two different inter-particle frictions and found that the peak stress ratio depended on the inter-particle friction. However, this conclusion is only valid for Oval II (with more elongated cross section), and there is a poor dependence for Oval I particles (with more rounded cross section). A detailed comparison is given by Fig. 9, including experimental data, simulation results and theoretical predictions. The DEM results include the simulations using various particle shapes: spherical, oval, polygonal and clumped particles. It is noted that the theoretical curve given by Horne [43] only considers the mobilized friction angle at the critical state, and the particle rotation effect is not considered. It is shown that his prediction only agrees well with the data at the low friction, while for high friction, the prediction significantly deviates from both experimental data and numerical simulation, which has been also discussed by Thornton [23]. The apparent discrepancy is largely attributed to the particle rolling effect, which can not be simply ignored, which is consistent with Peña et al. [22] and Alonso-Marroquín et al. [44], in which they used circular and polygonal particles respectively for the discrete element simulations. The independence of macroscopic shear resistance on inter-particle friction was explained by formation of rotational patterns in the particulate system [44]. Extremely, if inter-particle friction $\mu = 0$, the shear resistance is still available, which suggests that the inter-particle friction is not only the cause of macroscopic friction, but also the interlocking and particle structures, see [12,22,28,45].

6 Microscale observations

To examine potential microscopic mechanism underlying the mechanical response of granular soils described above, the 'sliding fraction', defined as the ratio of slipping contacts to the total, and the accumulated mean particle rotations of all particles, are introduced to quantify the particle sliding and rolling, respectively.

Slipping is assumed to be occurred at a contact if the tangential contact force is equal to the ultimate tangential force, which is determined by the normal contact force and inter-particle friction angle following the Coulomb's friction law [26]. Figure 10a–d show the relationship between the sliding fraction and the axial strain, and sliding fraction and stress ratio, against the inter-particle friction coefficients, for both drained and undrained tests respectively. It can be observed that the sliding fraction is highly dependent on the inter-particle friction angle, and the lower the friction angle, the higher is the sliding fraction. For example, under drained condition, the mean sliding fraction is almost 40 % for cases of $\mu = 0.05$ and 0.1, and decreases to 30 % when $\mu = 0.2$ and drops further to 10 % for $\mu = 0.5$ and a few percents for $\mu = 1.0$. This relationship between the sliding fraction and inter-particle friction angle emphasizes that the micro-scale particle sliding that is governed by the inter-particle friction angle is closely relevant to the macroscopic behavior of granular soils shown previously. It is also seen that for both drained and undrained tests, the development of the sliding fraction is closely related to the volumetric behavior of the samples, see Figs. 5, 6: the decrease of sliding fraction with ε_a or q'/p is co-occurred with the volume contraction (cases $\mu = 0.05$ and 0.1), while the increase of sliding fraction is echoed when the volume is dilatant but decrease when it is contracted (cases $\mu = 0.2$, 0.5 and 1.0).

For granular materials, the externally applied loading is transmitted by the force network via contacts of particles. The evolution of the microstructure engendered by loading can be characterized by the contact unit normal, branch vector as shown in Fig. 16 in the Appendix and Coordination Number (*CN*), defined as the mean contact numbers per particle for a granular assembly. Evaluation of the microstructure quantities and how they evolve under loading are given

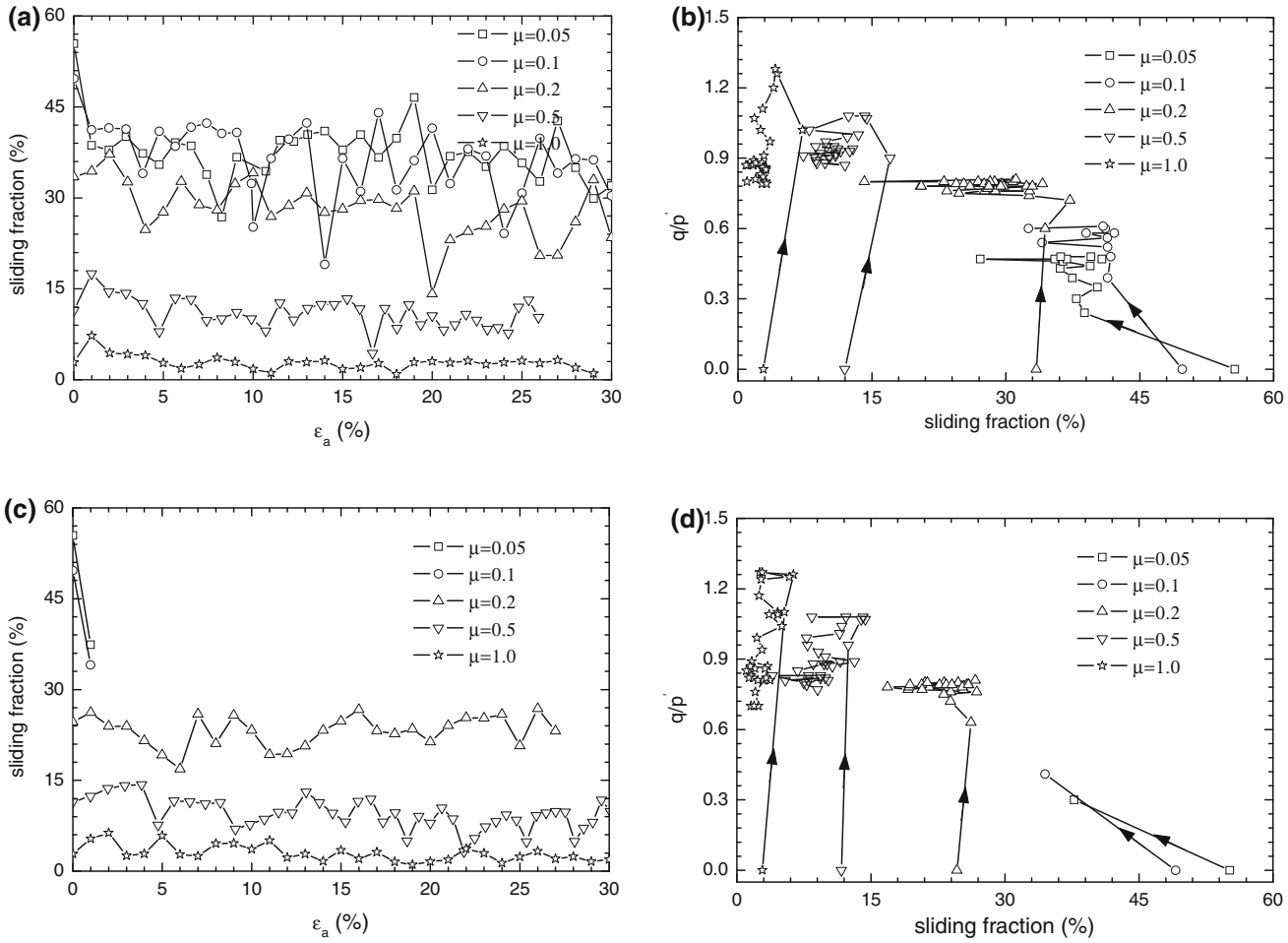

Fig. 10 Sliding contact fraction over various inter-particle frictions. **a**, **b** Drained tests; **c**, **d** undrained tests

in the Appendix. The internal force chains can be depicted by contact forces (both normal and tangential), mobilized friction coefficient, defined as the ratio of the local contact tangential force to the normal counterpart, and mean mobilized friction coefficient by averaging over all contacts among the assembly of particles.

Figure 11a presents the mean mobilized friction coefficient for various values of inter-particle friction under drained condition. It can be seen that the mean mobilized friction coefficients increase initially with the axial strain and then flatten off up to a certain axial strain (generally less than 2 %) for all μ values. However, the magnitudes of the mean mobilized friction coefficient are dependent on the inter-particle frictions. It shows that the maximum mean mobilized friction coefficients are 0.043 for $\mu = 0.05$ and 0.083 for $\mu = 0.1$, which are more than 80 % of the assigned inter-particle frictions, but they reduce to only 62 % for $\mu = 0.5$ (maxima = 0.309) and 44 % for $\mu = 1.0$ (maxima = 0.443), respectively.

Shown in Fig. 11b is the evolution of *CN* for various values of inter-particle friction under drained condition, and suggests that the lower friction may produce specimen with a larger *CN*, while the higher friction tends to give smaller *CN* by rearranging the particles via sliding and rolling. In general, *CN* is increased with decreasing inter-particle friction, as particle sliding is eased and particles packed more densely (see Fig. 10). The evolution of the *CN* values is closely related to the volumetric behavior of the specimens: *CN* increases initially with the axial strain up to a certain axial strain (generally less than 2 %) for all μ values, which is corresponding to the volume contraction of the specimens, and then flatten off for $\mu \leq 0.2$ but drop off nearly to a constant for $\mu \geq 0.5$ when the specimens dilate, although the specimens have similar initial void ratio of 0.15–0.17.

Figure 12 shows the evolution of anisotropy for these contact parameters during the shear loading. In general, the contact property evolves in a different manner as the inter-particle friction varies. As shown in Fig. 12a, in general, for cases with higher μ show greater anisotropy intensity Δ_d, and the increase of the shear strain will enhance the anisotropy intensity Δ. The anisotropy intensity may tend to flatten off at large strain for cases with higher μ, except

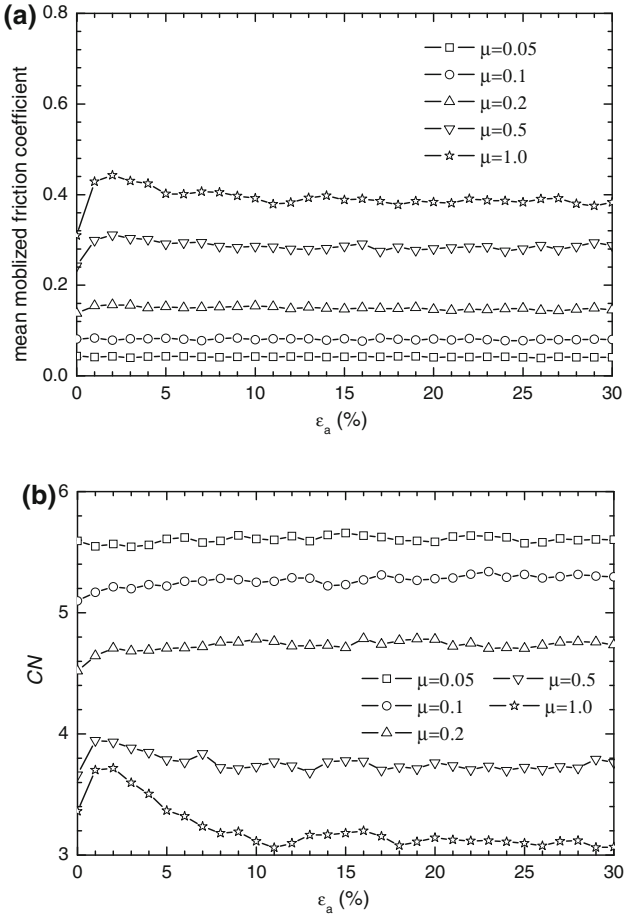

Fig. 11 Mobilized friction coefficient and coordination number with various inter-particle frictions for drained tests. **a** Mean mobilized friction coefficient; **b** *CN*

for case $\mu = 1.0$, which drops off and fluctuates after the peak. The numerical results are in accordance with existing experimental observations [46,47]: the concentration of the contact unit normals towards the major principal stress direction. Figure 12b, c give the evolutions of anisotropy intensities Δ_d^n and Δ_d^t for the contact normal and tangential forces respectively. As shown in the figure, except for $\mu = 1.0$, higher μ will give rise to higher Δ_d^n and Δ_d^t, which are also increasing with shear strain ε_a before flattening off in the large strain. It is also evident to see that higher μ tends to augment the anisotropic distributions of both the contact normal and tangential forces, such that results in a higher degree of induced structural anisotropy. A similar observation is also found in Fig. 12d, where the mobilized friction coefficient is computed as the ratio of local tangential force to normal force.

As an example, Fig. 13 illustrates the evolutions of the microstructures including the contact unit normal, contact normal and tangential forces, mobilized friction coefficient, and also contact force network at three featuring stages, i.e. initial, peak and ultimate states, for drained test with $\mu = 0.5$.

At initial state, both the contact normal and contact normal force show circular distributions while tangential force and mobilized friction coefficient are very small under isotropic stress state. The contact force chain formed by small and nearly circular grids has no apparent orientation, indicating that the sample is isotropic, which is also justified by the distributions of above four micro-scale variables.

At peak state, the principal directions of the contact parameters unanimously orient vertically, in response to the vertical deviatoric loading. There are a few sparse strong force chains in vertical direction along with dense vertical oriented grids. By comparison with those of initial state, at the peak state, more contacts are formed in the direction of major principal stress (vertical), while less contacts are in the minor principal stress direction (horizontal), making the contact unit normal distribution from being circular to elliptical vertically.

At ultimate state, the general distributions of contract parameters are similar to those at peak state. However, as shown in Figs. 5b, 12a, for $\mu = 0.5$, the behavior is strain softening after the peak state, while the evolution of contact normal anisotropy intensity Δ_d is increasing with the shear strain until ultimate state, such that the distribution of contact normal at the ultimate state is even more anisotropic than that at the peak state. Generally the stress ratio q/p' depends on the contact normal and contact force distributions in the micro-scale. If comparing the stress ratio distribution (Fig. 5b) with the contact force anisotropy (Fig. 12b, c), it is found that the stress ratio is more related to the contact force rather than contact unit normal. This observation is also supported by the DEM simulation results of Li [34].

It is also noted that the force chain formation is similar to the experimental results, in which the growth of force network by column-like structures are observed in the direction paralleled to the major principal stress direction, carrying and transmitting the deviatoric load [42,48,49].

For different inter-particle frictions, the contact unit normal distributions at various states are quite similar, but significant discrepancies are noted in the distributions of the contact forces, especially for the tangential force. Figure 14 presents the tangential force distribution at ultimate stage for $\mu = 0.05$, $\mu = 0.2$ and $\mu = 1.0$. It is seen that the magnitude of the contact tangential force is highly dependent on the inter-particle frictions, although their distribution patterns are similar. The major differences in the tangential forces may be the source of the different macroscopic behaviors including the dilatancy characteristics for different inter-particle friction stated previously. Figure 15 shows the corresponding contact force chains. The finer force network is developed for $\mu = 0.05$, while much coarser networks accompanied by larger pores can be observed for cases with larger frictions $\mu = 0.2$ and 1.0. This is consistent with the observations aforementioned that higher *CN* is for smaller inter-particle friction and vise versa.

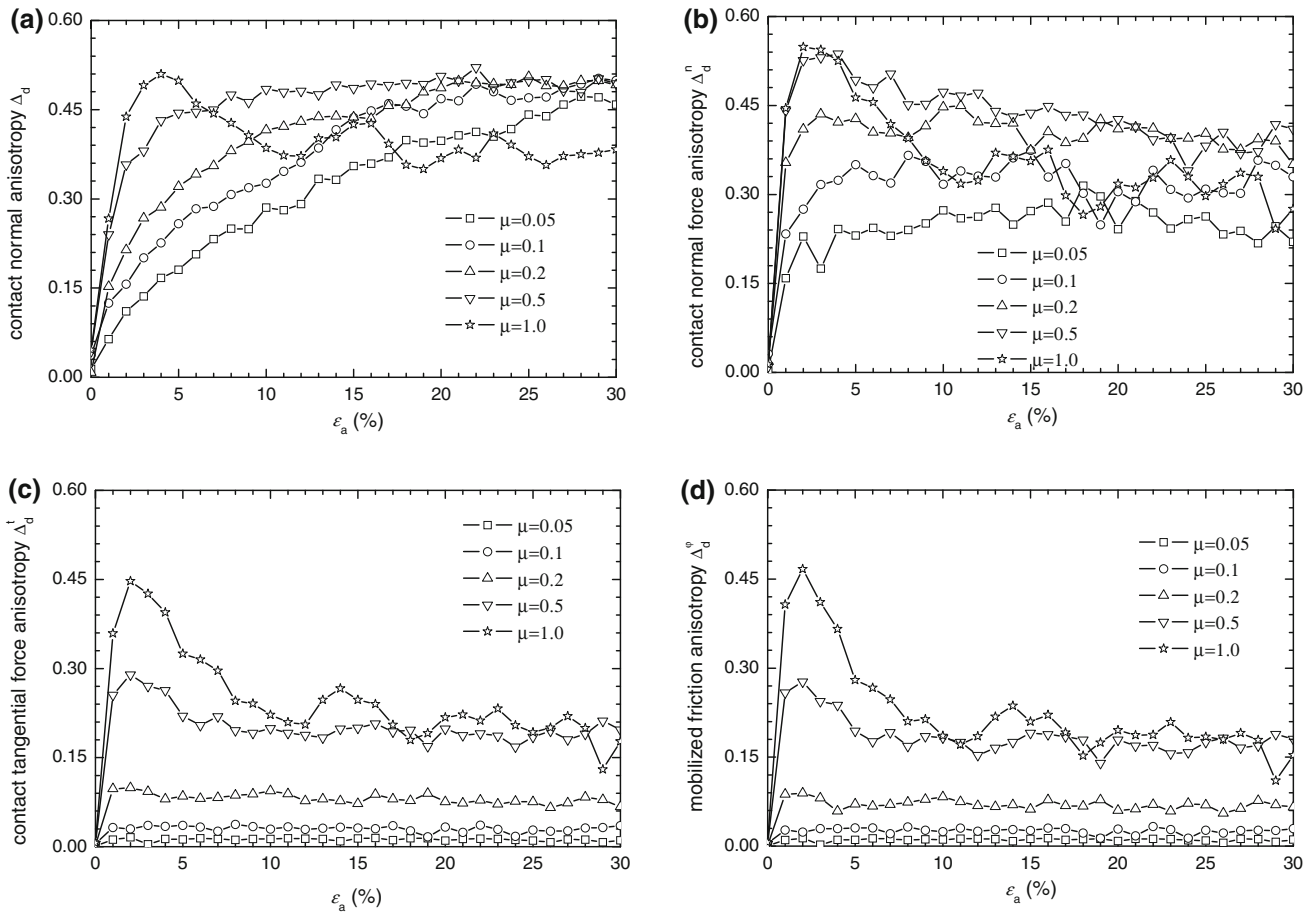

Fig. 12 Evolution of contact parameters' anisotropy with various inter-particle frictions for drained tests. **a** $\varepsilon_a \sim \Delta_d$, **b** $\varepsilon_a \sim \Delta_d^n$, **c** $\varepsilon_a \sim \Delta_d^t$, **d** $\varepsilon_a \sim \Delta_d^\phi$

7 Conclusions

This paper presents a systematic DEM analysis of the granular assembly sheared biaxially under both drained and undrained conditions. The samples all have similar initial isotropic fabric and density, and the same confining pressure, but with different inter-particle friction coefficient. The focus of this paper is placed on the interpretation of the mechanical behavior observed in the macro-scale by the microscopic analysis.

It is noted that the inter-particle friction significantly influences the mechanical behavior of the granular assembly, under both drained and undrained conditions. The increase of inter-particle friction brings the stress-strain response of the samples from hardening to softening, and a peak stress-ratio and strength are observed with higher frictions. However, the ultimate state stress ratio and strength are not appreciably affected by the inter-particle friction, which is consistent with previous investigations reported in the literature. Remarkably, it is noted that for a given stress ratio, the decrease of the inter-particle friction reduces the rate of dilation, which the famous Rowe's stress-dilatancy formulation fails to capture.

The striking overall behavior with varying inter-particle friction is interpreted by the interplay between the two forms of kinematics of the particles, sliding and rolling in the micro-scale. The strengths of samples with various inter-particle frictions appear to be influenced largely by the partitioning of deformation between inter-particle sliding and rolling, which is also helpful to explain the distinct distributions of *CN* and inter-particle forces. The anisotropic distribution of a number of contact parameters including contact unit normal, contact forces, and mobilized friction coefficient are identified and analyzed. The result shows that the different evolution patterns of contact anisotropy due to different inter-particle frictions can be linked with and interpret the observed macroscopic behavior.

Results presented in this paper lead to a better understanding of the role of inter-particle friction on the macro- and micro-mechanical behavior of the granular materials. Noting that the limitation of the two-dimensional analysis and ideal particle shape employed, validations with a

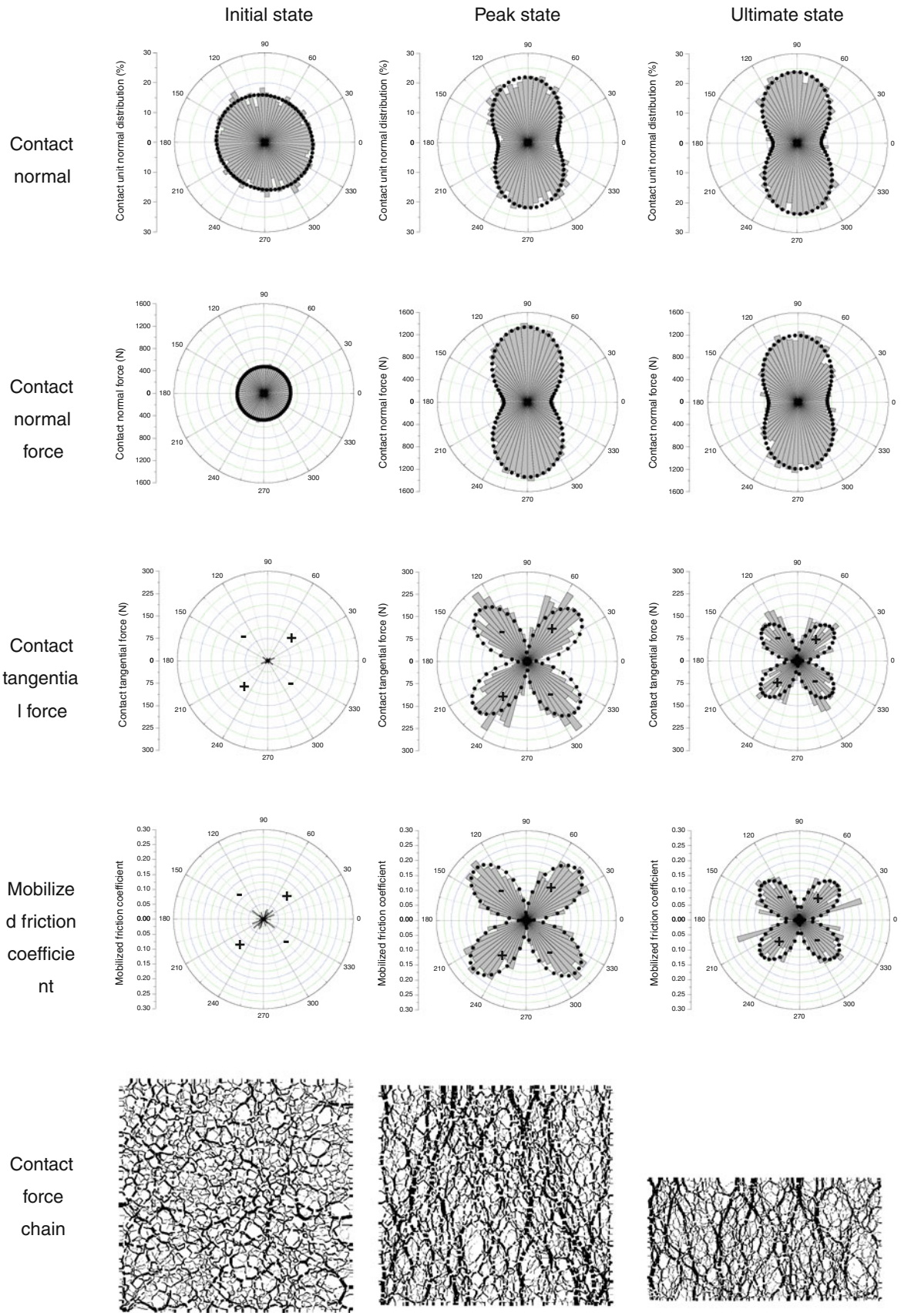

Fig. 13 Contact parameters' distribution for drained test with $\mu = 0.5$

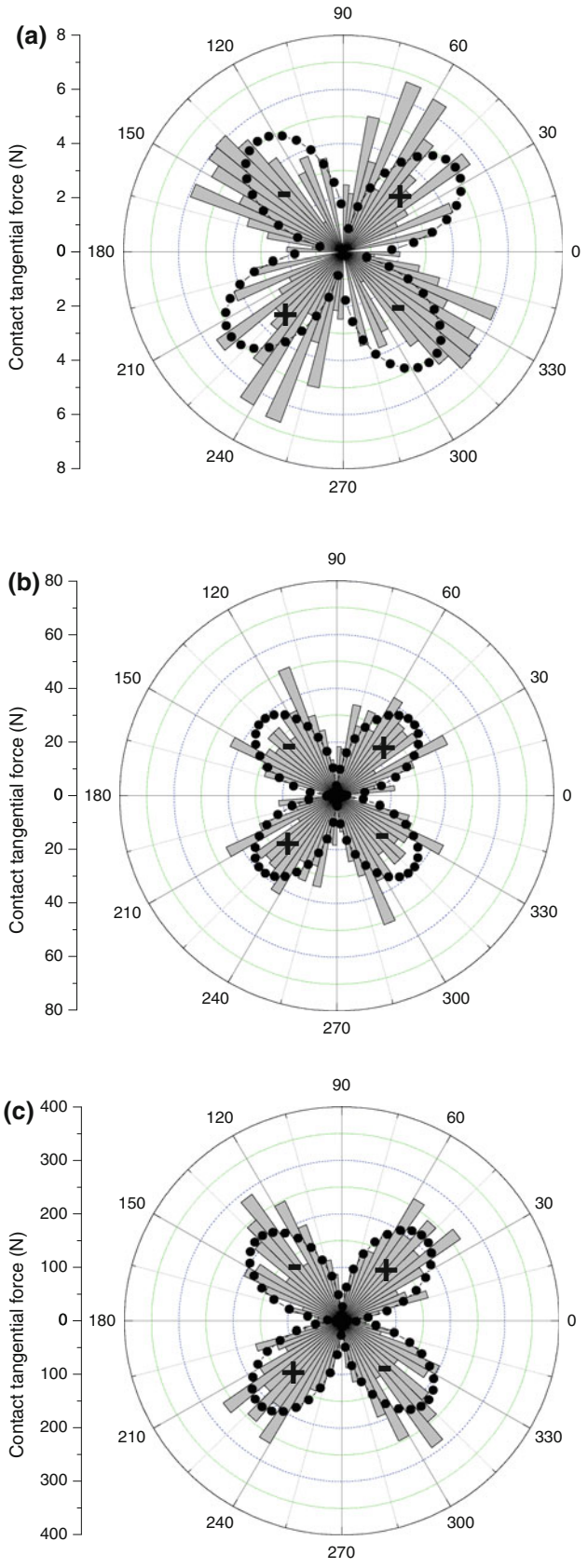

Fig. 14 Contact tangential force developed at ultimate state for drained test. **a** $\mu = 0.05$, **b** $\mu = 0.2$, **c** $\mu = 1.0$

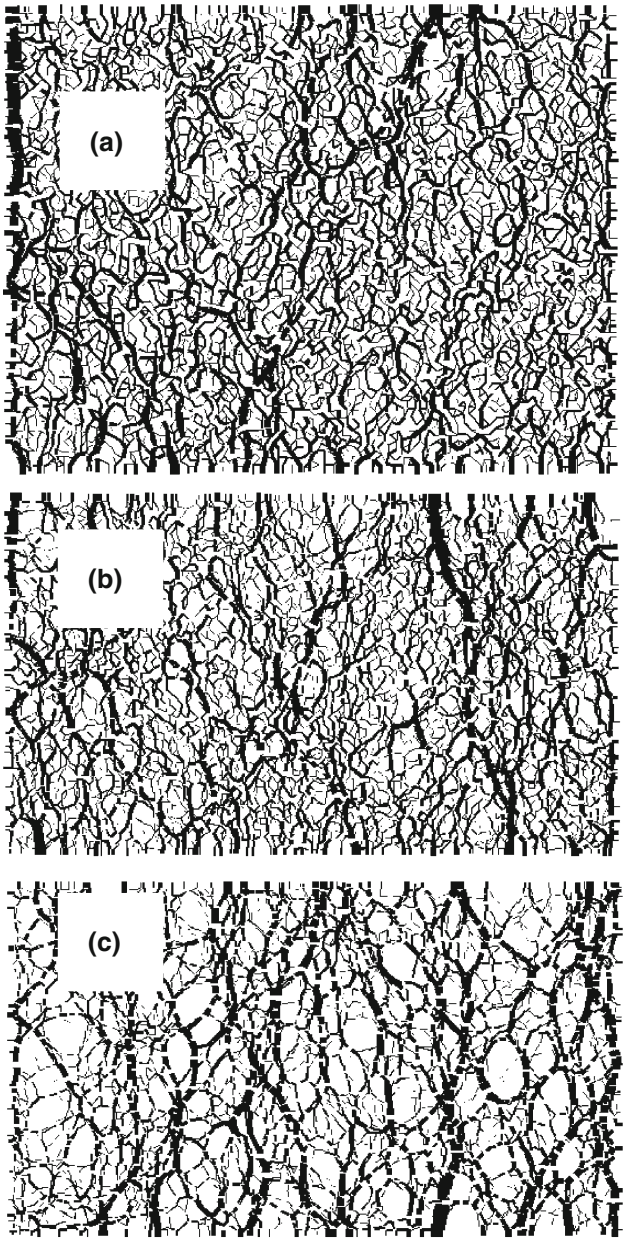

Fig. 15 Contact force network developed at ultimate state for drained test. **a** $\mu = 0.05$, **b** $\mu = 0.2$, **c** $\mu = 1.0$

three-dimensional model with more realistic particles would be required, to the development of the constitutive models addressing the influence of inter-particle friction in the light of the microstructure findings.

Acknowledgments The financial support provided by the Research Grants Council of Hong Kong (HKU 7191/05E) is acknowledged. The first author is also grateful for support by Natural Science Foundation of China (No. 50808159 & No. 51178421) and Fundamental Research Funds for the Central Universities (Program No. 2010QNA4028).

Appendix: Interpretation of micro-quantities

Anisotropy is an important feature for granular materials, and can be characterized mathematically by fabric tensors. The fabric tensors can be quantified by using the data registered during the numerical simulations in the micro-scale. Presently, the investigations are focused on the two-dimensional conditions. Figure 16 illustrates the representations for micro-quantities of two neighboring particles in contact. Referring to the work by Bathurst and Rothenburg [50], one may use the second-order form of Fourier series expansion to approximate the directional distribution of those micro-quantities. For quantities only having information in orientation (no information in magnitude), such as particle orientation, contact unit normal and branch vector orientation etc., the directional distribution in terms of the density function can be written in the form:

$$E(\varphi) = E_0(1 + d_{ij}n_i n_j) = E_0[1 + \Delta_d \cos 2(\varphi - \varphi_d)] \tag{A1}$$

where φ measures the orientation angle of an interested quantity with respect to the horizontal axis, ranging from 0° to 360°, $E_0 = 1/2\pi$ designates an isotropic distribution part, and Δ_d and φ_d are two parameters characterizing the intensity and principal direction of the anisotropic distribution of a particular quantity, and can be calculated through the components of d_{ij}, d_{11} and d_{12} (only two is sufficient in expressing the tensor d_{ij} because of its deviatoric and symmetric property), using the following relations:

$$\Delta_d = \sqrt{d_{11}^2 + d_{12}^2} \text{ and } \varphi_d = 1/2 \tan^{-1}(d_{12}/d_{11}) \tag{A2}$$

It is noted that Eq. (A1) gives the directional distribution of the quantities only having orientational information, while Eq. (A2) designates the anisotropy intensity and principal direction of such a distribution. It is noted that for an isotropic distribution, Δ_d vanishes.

However, a quantity r may likely possess the information of both the direction and magnitude at the same time, such as contact force, branch vector, contact vector, etc. Similar to Eq. (A1), a Fourier series approximation characterizing the spatial directional distribution of quantity r can be expressed into

$$r(\varphi) = r_0 \left[1 + \Delta_d^r \cos 2\left(\varphi - \varphi_d^r\right)\right] \tag{A3}$$

where r_0 represents an isotropic distribution over the directions and the pair of parameters Δ_d^r and φ_d^r are denoting the fabric anisotropy intensity and principal direction, and can be also obtained through the components of d_{ij} by using Eq. (A2).

It is aware that the local tangential force could be positive or negative, reflecting the sense of rotation imparted on the particle. The sign convention adopted here follows that positive tangential force tends to rotate a particle clockwise, and negative one means counter-clockwise. In this regard, the contact normal and tangential force directional distributions can be written as follows:

$$f_n(\varphi) = f_0 \left[1 + \Delta_d^n \cos 2\left(\varphi - \varphi_d^n\right)\right] \tag{A4}$$

$$f_t(\varphi) = -f_0 \Delta_d^t \sin 2\left(\varphi - \varphi_d^t\right) \tag{A5}$$

where f_0 represents an isotropic contact normal force and serves as a scaling factor for the tangential force distribution in Eq. (A5), and the subscripts/superscripts n and t denote normal and tangential respectively. In the meanwhile, the mobilized inter-particle friction could be defined as the ratio between the local contact tangential and normal forces. Its sign convention follows that of the tangential force, and may have positive or negative value as well, and approximately takes the same form as Eq. (A5) with subscript/superscript μ differentiated:

$$f_\mu(\varphi) = -\Delta_d^\mu \sin 2\left(\varphi - \varphi_d^\mu\right) \tag{A6}$$

As an effective numerical tool, DEM has the advantage of providing the direct information of the internal variables or quantities in the micro-scale, other than the conventional laboratory testing. Eqs. (A1) and (A4)–(A6) can visually present the spatial distributions of micro-quantities, and explicitly give the deviations from the corresponding isotropic distributions. Whenever a certain micro-quantity is isotropic, the components of its deviatoric fabric tensor should vanish.

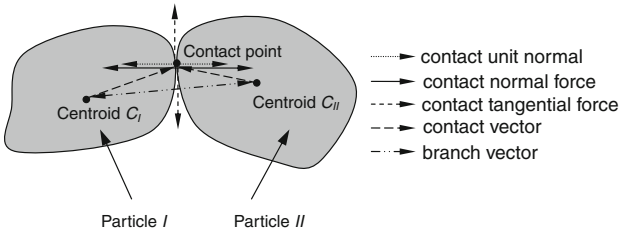

Fig. 16 Micro-quantities representation for two neighboring particles in contact

References

1. Arthur, J.R.F., Menzies, B.K.: Inherent anisotropy in a sand. Géotechnique **22**(1), 115–128 (1972)
2. Oda, M.: Initial fabrics and their relations to mechanical properties of granular materials. Soils Found. **12**(1), 17–36 (1972)
3. Bolton, M.D.: The strength and dilatancy of sands. Géotechnique **36**(1), 65–78 (1986)
4. Ishihara, K.: Liquefaction and follow failure during earthquakes. Géotechnique **43**(3), 351–415 (1993)
5. Yang, Z.X., Li, X.S., Yang, J.: Undrained anisotropy and rotational shear in granular soil. Géotechnique **57**(4), 371–384 (2007)

6. Yang, Z.X., Li, X.S., Yang, J.: Quantifying and modelling fabric anisotropy of granular soils. Géotechnique **58**(4), 237–248 (2008)
7. Cabalar, A.F., Clayton, C.R.I.: Some observations of the effects of pore fluids on the triaxial behaviour of a sand. Granul. Matter **12**(1), 87–95 (2010)
8. Santamarina, J.C., Cho, G.C.: Soil behaviour: the role of particle shape. In: Jardine, R.J., Potts, D.M., Higgins, K.G. (eds.) Advances in Geotechnical Engineering: The Skempton Conference, vol. 1, pp. 604–617. Thomas Telford, London (2004)
9. Mitchell, J.K., Soga, K.: Fundamentals of soil behaviour, 3rd edn. Wiley, NJ (2005)
10. Cavarretta, I.: The influence of particle characteristics on the engineering behaviour of granular materials. PhD Thesis, The University of London (2009)
11. Rowe, P.W.: The stress-dilatancy relation for static equilibrium of an assembly of particles in contact. Proc. R. Soc. Lond. Ser. A **269**(1339), 500–527 (1962)
12. Skinner, A.E.: A note on the influence of interparticle friction on the shearing strength of a random assembly of spherical particles. Géotechnique **19**(1), 150–157 (1969)
13. Haruyama, M.: Effects of surface roughness on the shear characteristics of granular materials. Soils Found. **9**(4), 48–67 (1969)
14. Procter, D.C., Barton, R.R.: Measurements of the angle of interparticle friction. Géotechnique **24**(4), 581–604 (1974)
15. Cavarretta, I., Coop, M., O'Sullivan, C.: The influence of particle characteristics on the behaviour of coarse grained soils. Géotechnique **60**(6), 413–423 (2010)
16. Chan, L.C.Y., Page, N.W.: Particle fractal and load effects on internal friction in powders. Powder Technol. **90**(3), 259–266 (1997)
17. Cho, G.C., Dodds, J., Santamarina, J.C.: Particle shape effects on packing density, stiffness, and strength: natural and crushed sands. J. Geotech. Geoenviron. Eng. **132**(5), 591–602 (2006)
18. Guo, P., Su, X.: Shear strength, interparticle locking, and dilatancy of granular materials. Can. Geotech. J. **44**, 579–591 (2007)
19. Jensen, R.P., Bosscher, P.J., Plesha, M.E., Edil, T.B.: DEM simulation of granular media-structure interface: effects of surface roughness and particle shape. Int. J. Numer. Anal. Methods Geomech. **23**, 531–547 (1999)
20. Nouguier-Lehon, C., Cambou, B., Vincens, E.: Influnece of paricle shape and angularity on the behavior of granular materials : a numerical analysis. Int. J. Numer. Anal. Methods Geomech. **27**, 1207–1226 (2003)
21. Peña, A.A., García-Rojo, G., Herrmann, H.J.: Influence of particle shape on sheared dense granular media. Granul. Matter **9**, 279–291 (2007)
22. Peña, A.A., Lizcano, A., Alonso-Marroquín, F., Herrmann, H.J.: Biaxial test simulations using a packing of polygonal particles. Int. J. Numer. Anal. Methods Geomech. **32**, 143–160 (2008)
23. Thornton, C.: Numerical simulations of deviatoric shear deformation of granular media. Géotechnique **50**(1), 43–53 (2000)
24. Powrie, W., Ni, Q., Harkness, R.M., Zhang, X.: Numerical modelling of plane strain tests on sands using a particulate approach. Géotechnique **55**(4), 297–306 (2005)
25. Alonso-Marroquín, F., Luding, S., Herrmann, H.J., Vardoilakis, I.: Role of anisotropy in the elastoplastic response of a polygonal packing. Phys. Rev. E **71**, 051304 (2005)
26. Suiker, A.S.J., Fleck, N.A.: Frictional collapse of granular assemblies. J. Appl. Mech. Trans. ASME **71**(3), 350–358 (2004)
27. Liu, S., Matsuoka, H.: Microscopic interpretation on a stress-dilatancy relationship of granular materials. Soils Found. **43**(3), 73–84 (2003)
28. Kruyt, N.P., Rothenburg, L.: Strength, dilatancy, energy and dissipation in quasi-static deformation of granular materials. In: García-Rojo, R., Herrmann, H.J., McNamara, S. (eds.) Powders and Grains, pp. 251. A.A. Balkema, Rotterdam (2005)
29. Cundall, P.A., Strack, O.D.L.: A discrete numerical model for granular assemblies. Géotechnique **29**(1), 47–65 (1979)
30. Jiang, M.J., Konrad, J.M., Leroueil, S.: An efficient technique for generating homogeneous specimens for DEM studies. Comput. Geotech. **30**(7), 579–597 (2003)
31. Feng, Y.T., Han, K., Owen, D.R.J.: Filling domains with disks: an advancing front approach. Int. J. Numer. Methods Eng. **56**(5), 699–713 (2003)
32. Bagi, K.: An algorithm to generate random dense arrangements for discrete element simulations of granular assemblies. Granul. Matter **7**(1), 31–43 (2005)
33. Cui, L., O'Sullivan, C.: Analysis of a triangulation based approach for specimen generation for discrete element simulations. Granul. Matter **5**(3), 135–145 (2003)
34. Li, X.: Micro-scale investigation on the quasi-static behavior of granular material. PhD Thesis, The Hong Kong University of Science and Technology (2006)
35. Huang, Z.Y., Yang, Z.X., Wang, Z.Y.: Discrete element modeling of sand behavior in a biaxial shear test. J. Zhejiang Univ. Sci. A **9**(9), 1176–1183 (2008)
36. Iwashita, K., Oda, M.: Rotational resistance at contacts in simulation of shear band development by DEM. J. Eng. Mech. ASCE **124**, 285–292 (1998)
37. Mahmood, Z., Iwashita, K.: Influence of inherent anisotropy on mechanical behavior of granular materials based on DEM simulations. Int. J. Numer. Anal. Methods Geomech. **34**(8), 795–819 (2010)
38. Fu, P., Dafalias, Y.F.: Study of anisotropy shear strength of granular materials using DEM simulation. Int. J. Numer. Anal. Methods Geomech. **35**(10), 1098–1126 (2011)
39. PFC2D User's manual, Itasca Consulting group, Inc., Minneapolis, USA (2005)
40. Ng, T.T.: Fabric evolution of ellipsoidal arrays with different particle shapes. ASCE J. Eng. Mech. **127**, 994–999 (2001)
41. Shodja, H.M., Nezami, E.G.: A micromechanical study of rolling and sliding contacts in assemblies of oval granules. Int. J. Numer. Anal. Methods Geomech. **27**, 403–424 (2003)
42. Oda, M., Konishi, J., Nemat-Nasser, S.: Experimental micromechanical evolution of strength of granular materials: effects of particle rolling. Mech. Mater. **1**(4), 269–283 (1982)
43. Horne, M.R.: The behaviour of an assembly of rotund, rigid, cohesionless particles III. Proc. R. Soc. Lond. Ser. A **310**(1500), 21–34 (1969)
44. Alonso-Marroquín, F., Vardoulakis, I., Herrmann, H.J., Weatherley, D., Mora, P.: Effects of rolling on dissipation in fault gouges. Phys. Rev. E **74**, 031306 (2006)
45. Cambou, B.: From Global to Local Variables in Granular Materials, Thorton, Editor, Powders & Grains. pp. 73–86. Balkema, Rotterdam (1993)
46. Drescher, A.: An experimental investigation of flow rule for granular assemblies. Géotechnique **26**(4), 49–65 (1976)
47. Oda, M., Konishi, J., Nemat-Nasser, S.: Some experimentally based fundamental results on the mechanical behaviour of granular materials. Géotechnique **30**(4), 479–495 (1980)
48. Oda, M., Kazama, H.: Microstructure of shear bands and its relation to the mechanisms of dilatancy and failure of dense granular soils. Géotechnique **48**(4), 465–481 (1998)
49. Oda, M.: The mechanism of fabric changes during compressional deformation of sand. Soils Found. **12**(2), 1–18 (1972)
50. Bathurst, R.J., Rothenburg, L.: Investigation of micromechanical features of idealized granular assemblies using DEM. Eng. Comput. **9**, 199–210 (1992)